Dynamic Light Scattering from Semidilute Suspensions of fd Virus[1]

S. Fujime,* M. Takasaki-Ohsita, and T. Maeda

Mitsubishi-Kasei Institute of Life Sciences, Machida, Tokyo 194, Japan.
Received November 3, 1986

ABSTRACT: Bacteriophage fd is a semiflexible filament whose contour length (L) is 895 nm and diameter is 9 nm. Dynamic light scattering spectra from monodisperse suspensions of fd at cL^3 up to 160 (cL^3 being the number of fd in a volume L^3) were analyzed, and it was concluded that the Brownian motions in lengthway and sideway translation as well as flexion are almost free, whereas the rotational Brownian motion is clearly restricted at high cL^3. A long-tail behavior of the spectra at high cL^3 was qualitatively discussed with an empirical formula.

Introduction

In a recent paper,[1] we presented dynamic light scattering spectra of monodisperse suspensions of very long and semiflexible rods, bacteriophage fd, in the dilute and semidilute regimes. This phage is 895 nm in length (L) and 9 nm in diameter (d). On the basis of our theory for the dynamic light scattering spectrum for a weakly bending rod,[2,3] the spectra at a dilute regime were successfully analyzed to give a flexibility parameter of $\gamma L = 0.23$, where γ is the inverse of the statistical (or the Kuhn) length.[1] In this report, we attempt to analyze spectra from suspensions of this phage in the semidilute regime.

Even for semidilute suspensions of *rigid* rods, the polarized light scattering spectrum has not yet been fully characterized up to now. This difficulty is due partly to the fact that none of the very long rods so far studied is truly rigid and partly to the simultaneous contributions from translational and rotational motion. In such a situation, we discuss the polarized light scattering spectrum from monodisperse suspensions of weakly bending filaments in the semidilute regime. Therefore, our study is inevitably semiquantitative. This work is a supplement to ref 1, and in what follows Figure I-3, for example, refers to Figure 3 in ref 1. Although details of the experimental and numerical procedures have been given elsewhere,[1-4] a short summary of the theoretical background is given below for the convenience of discussion and for the introduction of terminology.

The field correlation function $G^1(\tau)$ of light scattered from a dilute and monodisperse suspension of semiflexible and long filaments is a function of K (the length of the scattering vector), D_1 and D_3 (translational diffusion coefficients perpendicular and parallel to the rod axis, respectively, with $D_0 = (2D_1 + D_3)/3$ being the overall translational diffusion coefficient), Θ (the end-over-end rotational diffusion coefficient), and γ. The unnormalized form of $G^1(\tau)$ is given by

$$G^1(\tau) = G_D(\tau)F(K,\mu^2,\Theta,\gamma;\tau) \quad (1)$$

$$G_D(\tau) = \exp[-(D_0 - (D_3 - D_1)/3)K^2\tau] \equiv \exp(-D_1K^2\tau) \quad (2)$$

where $\mu^2 = (D_3 - D_1)K^2/\Theta$ and $F(K,\mu^2,\Theta,\gamma;\tau)$ is expressed by a threefold integration, whose explicit expression is found elsewhere.[1,2] Although not explicitly indicated in eq 1, $F(...)$ depends also on T (absolute temperature), η (solvent viscosity), L, d, and so on. By definition of the first cumulant $\bar{\Gamma} = -\lim d[\ln G^1(\tau)]/d\tau$, where "lim" means taking the limiting value of its operand at $\tau = 0$, we have a simple expression for the initial decay rate of $G^1(\tau)$ as

$$\bar{\Gamma}/K^2 = D_0 + (L^2/12)\Theta f_1^*(k) + (D_3 - D_1)[f_2^*(k) - 1/3] + \sum_m D_{[m]}a_m(k) \quad (3)$$

where $D_{[m]} = (k_BT/4\pi\eta L)(1 + f_m)$ is the diffusion coefficient of the m-th bending mode of the semiflexible rod ($m \geq 2$); an explicit form of the hydrodynamic interaction term, f_m, is found elsewhere.[3] $f_1^*(k)$, $-[f_2^*(k) - 1/3]$ and $a_m(k)$ ($m \geq 2$) are functions of both $k = KL/2$ and γ, and they are zero at $k = 0$ and monotonically increase with k; the limiting values are $f_1^* = 1$, $-[f_2^* - 1/3] = 1/3$, and $a_m = 1$ as $k \to \infty$. Their explicit forms are found elsewhere.[2] In the right-hand side of eq 3, the first term comes from the overall translational diffusion, the second term from the rotational diffusion, the third term from anisotropy in translational diffusion, and the fourth term(s) from bending motions. For a rigid rod, the last term(s) in eq 3 does not appear.[4]

The dynamic light scattering spectrum from a semidilute suspension of monodisperse rigid rods was first considered by Doi and Edwards (DE).[5] In the framework of the DE model, $G^1(\tau)$ for a semidilute suspension of rigid rods can be computed by use of a formula for a dilute suspension including anisotropy in translation ($\mu^2 \neq 0$),[4] *if we put*

$$D_{c,1} = \beta' D_1, \qquad D_{c,3} = D_3, \qquad \Theta_c = \beta\Theta \quad (4)$$

where D_i and Θ with and without the subscript c are those in the semidilute and dilute regimes, respectively. The dilute suspension values of D_i ($i = 1$ and 3) and Θ are found elsewhere.[1] In the DE model, $\beta' = 0$ and $\beta \sim (cL^3)^{-2}$, where cL^3 is the number of rods in volume L^3. However, we treat here both β' and β to be adjustable parameters (≤ 1) depending on cL^3. Equations 1-3 can also be extended to the case of a semidilute suspension of semiflexible filaments by simply replacing D_i and Θ with $D_{c,i}$ and Θ_c, respectively.[2] As discussed below, however, eq 2 after this simple replacement is valid only for the short-τ behavior of $G^1(\tau)$. An alternative to eq 2 for high cL^3 will be discussed later.

Results and Discussion

Figure 1 shows some examples of the profiles of correlation functions. As the fd concentration (hereafter denoted by [fd] in mg/mL and/or $cL^3 = 26.2$[fd]) increased, a long tail of the correlation function appeared (see also Figure I-8). Figure 2 shows the results of the third-order cumulant expansion of the correlation functions at different cL^3. The $\bar{\Gamma}/K^2$ values in Figure 2 are larger than the corresponding values in Figure I-7, mostly because the second-order cumulant expansion was applied in the latter, where the very short-τ portion of the correlation function with a long tail could not be well fitted (see also the caption to Figure 2).

To roughly observe contributions to $\bar{\Gamma}/K^2$ from various modes of motions, we first computed eq 3 for $\gamma L = a_m(k) = 0$ (rigid rod). $\bar{\Gamma}/K^2$ values are shown in Figure 2 by dashed ($\beta = \beta' = 1$) and dotted ($\beta = 0$ and $\beta' = 1$) lines. Most of the experimental points lie above the dashed line,

0024-9297/87/2220-1292$01.50/0

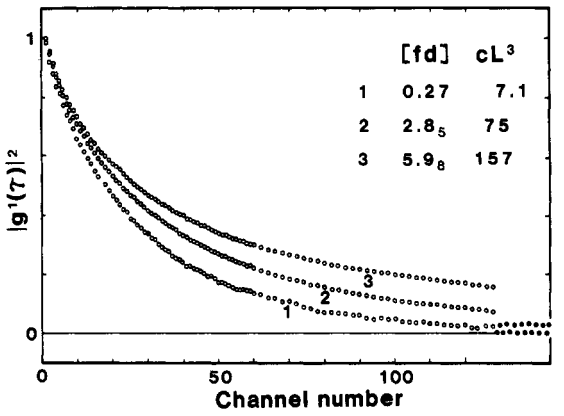

Figure 1. Some examples of net correlation functions $|g^1(n\Delta\tau)|^2$ for suspensions of the fd virus at a scattering angle of 90°, 24 °C, and a channel delay time $\Delta\tau = 7.0$ μs. Every second point was displayed after the sixtieth channel. Filled circles show extra channels starting from $\tau = 512\Delta\tau$. The upper set for curve 3 and lower set for curve 1. $cL^3 = 26.2$[fd], where c is in rods/mL and [fd] in mg/mL.

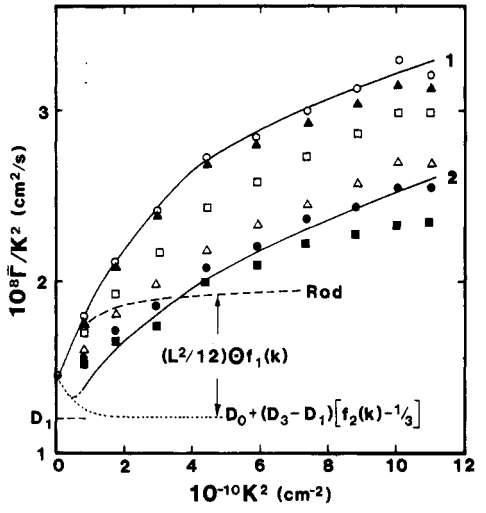

Figure 2. $\bar{\Gamma}/K^2$ vs. K^2 relationships for suspensions of the fd virus. To obtain these $\bar{\Gamma}/K^2$ values, we made use of the third-order cumulant expansion formula and a weight function $w_n = [g^1(n\Delta\tau)]^4$ in a least-squares fit. This heavy weight for small n was essential to obtain a good fit over the entire portion of $|g^1(n\Delta\tau)|^2$ having a long tail as shown in Figure 1, otherwise a poor fit was observed at the initial portion of the decay. The $\bar{\Gamma}/K^2$ values were T/η-corrected to 5 °C. [fd]s were 0.088 mg/mL ($cL^3 = 2.3$) for (○), 0.27 (7.1) for (▲), 1.3_2 (35) for (□), 2.8_5 (75) for (△), 3.9_5 (103) for (●), and 5.9_8 (157) for (■). The solvent was 150 mM KCl and 15 mM phosphate buffer (pH 7.0). The dashed and dotted lines show respectively the rigid-rod values of $\bar{\Gamma}/K^2$ and $D_0 + (D_3 - D_1)[f_2(k) - {}^1/_3] \equiv D_1 + (D_3 - D_1)f_2(k)$, and hence the difference between dashed and dotted lines shows $(L^2/12)\Theta f_2(k)$, where $f_i(k)$ are the rigid-rod values of $f_i{}^*(k)$. Theoretical $\bar{\Gamma}/K^2$ were for D_i, $\gamma L = 0.23$, and Θ with $\beta = \beta' = 1$ (the solid line 1) and $\beta = 0.02$ and $\beta' = 1$ (the solid line 2), where D_i and Θ were their dilute suspension values. For details, see text.

indicating that the contribution to $\bar{\Gamma}/K^2$ from bending motions is substantial also at high cL^3. Next, eq 1 was computed for $\gamma L = 0.23$, and the resultant $G^1(\tau)$s were analyzed by use of the same program as for the experimental correlation functions (for the details of computation, see Numerical Method in ref 1). The $\bar{\Gamma}/K^2$ values thus obtained are shown by solid lines 1 ($\beta = \beta' = 1$) and 2 ($\beta = 0.02 \sim 0$ and $\beta' = 1$) in Figure 2. Most of the experimental points lie between lines 1 and 2, suggesting that experimental data for any cL^3 studied so far can be fitted mostly by adjusting only a β value appropriate to each cL^3. (Numerical values of D_i, Θ, and γL in the theoretical computation here and hereafter were fixed to their dilute suspension values, unless otherwise stated. Adjustable parameters were then β' and β in eq 4 and A in eq 5 given later.)

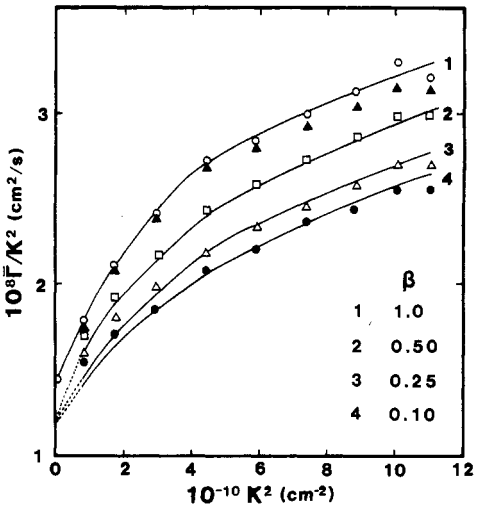

Figure 3. $\bar{\Gamma}/K^2$ vs. K^2 relationships. For symbols for the experimental points, see the caption to Figure 2. The theoretical curves were obtained for dilute suspension values of D_i, Θ, $\gamma L = 0.23$, and varied β.

Figure 3 shows the $\bar{\Gamma}/K^2$ vs. K^2 relationships from the computed results of eq 1 for $\beta' = 1$ and varied β. The simulation of $\bar{\Gamma}/K^2$ seems to be satisfactory at high K^2. However, the theoretical lines for $\beta < 1$ deviate from the experimental points at low K^2 and seem to tend toward $\sim 1.2 \times 10^{-8}$ cm²/s at $K^2 = 0$; i.e., $D_1 = 1.19 \times 10^{-8}$ cm²/s; note $G_D(\tau) = \exp(-D_1K^2\tau)$ in eq 2. This behavior is due to the effect of anisotropy in translational diffusion of a long rod and can be easily understood by examining the theoretical lines in Figure 2.

As seen in Figure I-4, the $\bar{\Gamma}/K^2$ at $K^2 = 9.48 \times 10^8$ cm^{-2} (this K^2 is small enough to evaluate D_0) substantially increases with [fd]. (A notable increase in D_0 with cL^3 has been reported, for example, for PBLG in DMF.[6,7]) Although measurements of $\bar{\Gamma}/K^2$ at this K^2 were made only up to [fd] = 2 mg/mL, we made a linear extrapolation of $\bar{\Gamma}/K^2$ up to as high as 6 mg/mL to estimate D_0 values at high [fd]s. The extrapolated values of $\bar{\Gamma}/K^2$ are shown in brackets [ ] in Figure 4. Using these values as $*D_0$, we evaluated $*D_1$ (with $\beta' = 1$) and $*D_3$ for each [fd]; we simply assumed $*D_i = \alpha D_i$ for $i = 0$, 1, and 3 (the asterisk denotes the quantity at [fd] $\neq 0$, and hereafter it is omitted because we used eq 4 again for these $*D_i$). By use of the newly evaluated D_i instead of their dilute suspension values, eq 1 was recomputed for varied β (and β') values. The results are shown in Figure 4, where the simulation seems to be satisfactory over the entire range of K^2 studied so far.

Here we have to discuss some details of our analysis given in Figure 4. The vertical bars (curve 1) in Figure 5 show the range of β values that could reasonably simulate experimental data at each cL^3. Up to this stage, we focused our attention on the initial decay rate $\bar{\Gamma}/K^2$ alone. However, as seen from $G_D(\tau) = \exp(-D_1K^2\tau)$ in eq 2, the computed correlation function did not show as long a tail as experimental ones in Figure 1. If we assumed $\beta' = 0.5$, for example, in order to ensure the long tail, the initial value of the decay did not match that of the observed one. Then we had to seek an alternative to eq 2, at least, to a first-order approximation.

Pusey has proposed an expression of $G^1(\tau)$ for a concentrated suspension of "highly charged" spheres inter-

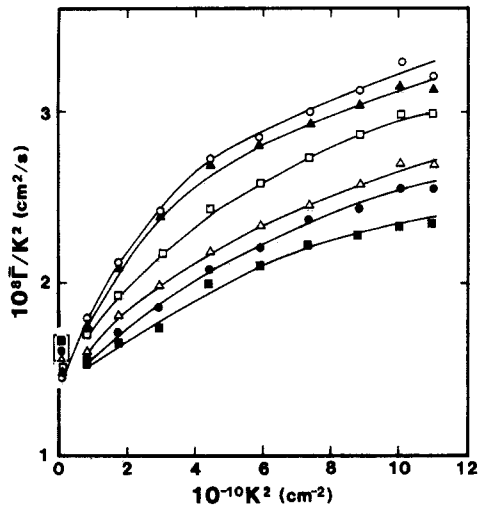

Figure 4. $\bar{\Gamma}/K^2$ vs. K^2 relationships. For symbols for experimental points, see the caption to Figure 2. The experimental points at the lowest K^2 were obtained by linear inter- (○, ▲, □) and extrapolation (△, ●, ■) of observed points given in Figure I-4. From these estimated values of $\bar{\Gamma}/K^2$ (=$^*D_0$), $^*D_1$ (with β' = 1) and $^*D_3$ were evaluated for each cL^3. With these $^*D_i$ values and the dilute suspension values of Θ and γL = 0.23, theoretical curves were obtained; the range of β values giving reasonable fit are shown in Figure 5. For more details, see text.

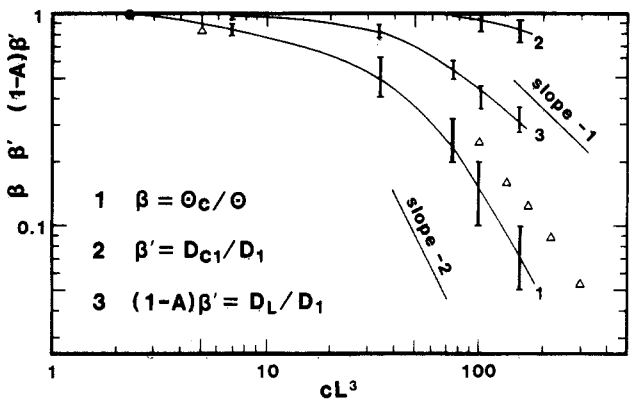

Figure 5. β, β' and $(1 - A)\beta'$ vs. cL^3 relationships. $\beta = \beta' = 1$ and $A = 0$ are assumed for [fd] = 0.088 mg/mL (●). For a comparison, triangles show β values obtained from transient electric birefringence measurements for this virus.[11]

acting strongly with each other,[8] a simple analogy to which gives

$$G_D(\tau) = \exp[-D_1K^2\{(1 - A)\tau + (A/\lambda)(1 - \exp(-\lambda\tau))\}] \quad (5)$$

$$\lambda = 2D_1K^2 \quad (6)$$

where $0 \le A < 1$ (this "A" is equal to Pusey's A/λ). $G_D(\tau)$ in eq 5 tends toward $\exp(-D_1K^2\tau)$ for $\tau \ll \lambda^{-1}$ and $\exp[-D_1(1 - A)K^2\tau]$ for $\tau \gg \lambda^{-1}$. The factor 2 in the expression of λ may be parameterized, but we fixed it in order to reduce the number of unknowns. The parameter A may have a certain relation with the cage size or the average number of neighbors; for high values of cL^3, the A values are larger. Then, a properly chosen A value for each cL^3 (except for the highest two) gave a good agreement between profiles of computed and experimental correlation functions over the entire range of delay times and at any K^2 so far studied; A= 0.0, 0.05, 0.15, and 0.45 for cL^3 = 2.3, 7.1, 35, and 75, respectively. At the highest two cL^3s, the D_1 value in eq 5 and 6 had to be reduced ($\beta' < 1$). We obtained A = 0.55 and β' = 0.9 for cL^3 = 103 and A = 0.6 and β' = 0.8 for cL^3 = 157. The parameter A was indeed

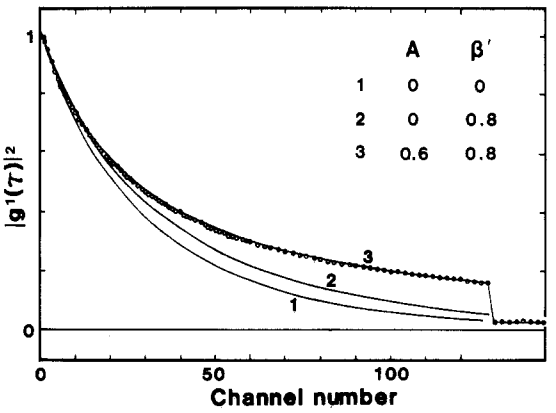

Figure 6. Comparison of the profiles of experimental and computed correlation functions at the scattering angle of 90° and at [fd] = 5.9_8 mg/mL (cL^3 = 157).

insensitive to K^2. Figure 6 shows the profiles of simulated correlation functions at cL^3 = 157 and at the scattering angle of 90°, where the initial decay of the line 2 is very close to that of the line 3; use of eq 5 with a nonzero A affected $\bar{\Gamma}/K^2$ values very little. The range of the β' values is also given in Figure 5 for each cL^3. A possibility cannot necessarily be excluded that this slight dependence of β' on cL^3 is due to an overestimation of $\bar{\Gamma}/K^2$ at the lowest K^2 by extrapolation to a too high cL^3. Let D_L be the translational diffusion coefficient at a long-τ region. Then, eq 5 give $D_L/D_1 = (1 - A)\beta'$, of which a value for each [fd] is also given in Figure 5.

Now, we would like to discuss the *rationale* of our empirical treatments.

1. To consider the motion of a test rod in a semidilute suspension, let us imagine a cage formed by surrounding rods. Since the volume occupied by one particle is given by $1/c \sim a_c^2L$, we have a cage radius $a_c \sim L/(cL^3)^{1/2}$.[4,10] For cL^3 = 66, we can estimate $a_c \sim$ 110 nm. This size of a_c should be compared with $1/K$; i.e., a_cK = 110/110 and 110/40 (nm/nm) at the scattering angles of 30° and 90°, respectively. The correlation time τ_c of the K component of free sideway translation is given by $\tau_c = (D_1K^2)^{-1}$, during which time the center-of-mass travels a distance u; $\langle u^2\rangle_1 = 2D_1\tau_c = 2/K^2$ or $\langle u^2\rangle_1K^2 = 2$. Then we have $a_c^2 \ge \langle u^2\rangle_1$ except for small K^2. Namely the space inside the cage is large for very long rods, and the sideway translation is expected to be almost free; $\beta' \sim 1$. (At the lowest K^2, $1/K$ = 320 nm so that β' might be small. Even for $\beta' \sim 0$, $G^1(\tau)$ at this K^2 will decay with a decay rate $D_3K^2/3$; see eq 3.) On the other hand, for short rods such as L = 100 nm, we have a_c = 12 nm for cL^3 = 66; the space inside the cage is very narrow, resulting in strongly restricted sideway translation, $\beta' \ll 1$.[5]

2. From the relationship $\langle\delta_m^2\rangle = 2D_{[m]}\tau_m$, where $D_{[m]}$ is in eq 3 and τ_m is the relaxation time of the m-th bending mode, the root-mean-square amplitude of the lowest mode of the bending motion, $\langle\delta_2^2\rangle^{1/2}$, is estimated to be less than 60 nm for the fd virus.[1-3] This size is smaller than the size of the cage; the bending motion is also expected to be almost free in the cage. For a given scattering angle, say 90°, differences between the observed $\bar{\Gamma}/K^2$ and the computed $D_0 + (L^2/12)(\beta\Theta)f_1(k) + (D_3 - D_1)[f_2(k) - {}^1/_3]$ with β values of ours or in the literature (Figure 5) are almost independent of cL^3, suggesting again almost free bending motions (or almost no dependence on cL^3 of the fourth term(s) in eq 3) up to cL^3 = 160.[9]

3. There are several experimental and theoretical studies on the rotational motion of rigid rods in semidilute suspensions,[10-15] all of which have shown much weaker cL^3

dependence of β than that in the initial DE model.[5]

4. The short-time ($\tau \ll \tau_c$) behavior of $G^1(\tau)$ can be described well with eq 1 and 2 with varied β. On the other hand, the long-time ($\tau \gg \tau_c$) behavior of $G^1(\tau)$ can be described with eq 1 and 5 with varied A and β. Because the structure of $F(...)$ in eq 1 is quite insensitive to μ^2 for $\mu^2 \geq 50$,[4] or $K^2 \geq 1 \times 10^{10}$ cm^{-2} in the present case (note that the dotted line in Figure 2 reaches its almost final value at $K^2 = 1 \times 10^{10}$ cm^{-2}), a memory effect on the translational motion appears only through $G_D(\tau)$ in the present interest of the K^2 range. Therefore, simple replacement of eq 2 with eq 5 will be allowed provided eq 5 is applicable to our case. Equation 5 has been derived for a situation that the test particle is temporarily trapped in a repulsive cage formed by its neighbors.[8] The repulsive interaction may express our situation that the test particle is hard to freely come close to its neighbors. The "collision time" $\tau_I = \lambda^{-1}$ in ref 8 is defined by the time taken by the test particle to move a reasonable fraction of the mean interparticle spacing. Then, we may put $\tau_I \sim \tau_c$. The factor 2 in eq 6 was chosen a posteriori to fit the data.

There were many parameters in order to describe dynamic light scattering spectra of semiflexible filaments in the semidilute regime, such as β' (or $D_{c,1}$), α (in $^*D_0 = \alpha D_0$), β (or Θ_c), γ, and A (in eq 5). The α value of each cL^3 was determined for the $\bar{\Gamma}/K^2$ value at the lowest K^2. The value of $\gamma L = 0.23$ was assumed independently of cL^3. We first computed $F(...)$ in eq 1 for $\beta' = 0$ and varied β, and then $G^1(\tau)$ for varied A (and β' at the highest two cL^3s) to obtain fitting in its profile with the observed one, and finally $\bar{\Gamma}/K^2$. We have considered the long-term memory effect only on $G_D(\tau)$ in eq 5 but not on $F(...)$ in eq 1. Furthermore, eq 5 with eq 6 has no firm physical basis in our case. At the moment, our treatments may be nothing more than simple curve fitting. Therefore, we do not argue that the sizes of the parameters obtained from simulation are absolute; at the present degree of quantitativeness, it is not clear whether β and $(1 - A)\beta'$ behave similarly to each other against cL^3. Nevertheless, we would like to suggest the following:

1. Both β' and γL are very weakly dependent on cL^3 in the case of very long filaments, at least, up to $cL^3 = 160$ so far studied.

2. β changes against cL^3 nearly as predicted by current theories for rigid rods.[13-15]

3. D_L/D_1 seems to change with cL^3 more or less similarly to what β does.

4. In the case of highly charged spheres at very low ionic strength, the decay constant λ in eq 5 is reported to be very insensitive to K^2.[8] On the other hand, the fact that eq 5 with eq 6 worked well over a wide range of K^2 suggests that a steric hindrance is a major source of the interfilament interaction in our case.

Finally, we would like to suggest a possibility. For PBLG ($L = 206$ nm) in DMF, $\bar{\Gamma}$ vs. K^2 relationships have been presented.[7] At a low concentration (0.25 mg/mL or $cL^3 = 4.4$), there is an *upward* curvature beginning at $K^2 \sim 4 \times 10^{10}$ cm^{-2} in the $\bar{\Gamma}$ vs. K^2 relation. At high concentrations (23 mg/mL or $cL^3 = 400$ and 14.8 mg/mL or $cL^3 = 260$), on the other hand, there are *downward* curvatures beginning at $K^2 \sim 3 \times 10^{10}$ cm^{-2}. These curvatures could be fitted almost quantitatively by eq 3 for $\gamma L = 0$, the upward curvature by the use of $\bar{\Gamma}/K^2 = D_0 + (L^2/12)\Theta f_1(k) + (D_3 - D_1)[f_2(k) - {}^1/_3]$ for dilute solution values of D_i and Θ, and downward curvatures by the use of $D_1 = \Theta = 0$ ($\beta' = \beta = 0$) and the observed value of $^*D_0$ ($=^*D_3$), namely $\bar{\Gamma}/K^2 = {}^*D_3 f_2(k)$ (note that $f_2(k)$ decreases from ${}^1/_3$ at $k = 0$ to zero at $k = \infty$; see also the initial portions of the dashed and dotted lines in Figure 2).

Concluding Remarks

Our method of analysis discussed above seems promising in elucidating the dynamics of very long and slightly bending filaments in the semidilute regime. Important problems which will be studied in the future are (1) to give a firm physical basis to eq 5 and 6, or to derive their alternatives; (2) to examine the memory effect also on $F(...)$ in eq 1, in this particular case, a possible memory effect on flexing motions of filaments; (3) to measure the intensity correlation function $G^2(\tau)$ at variously spaced delay times in order to examine both short- and long-τ behaviors of $G^2(\tau)$ more precisely at high cL^3, which is crucial to test the theoretical formulation; (4) to apply the inverse Laplace transformation to such correlation functions as in (3) to extract a distribution of relaxation times. The distribution of relaxation times will provide more crucial information for a test of various theoretical formulations than the first cumulant does. All of these problems are now under consideration.

Acknowledgment. This work was partially supported by a Grant-in-Aid from the Ministry of Education, Science and Culture of Japan.

References and Notes

(1) Maeda, T.; Fujime, S. *Macromolecules* **1985**, *18*, 2430; correction to typographical errors is in: *Macromolecules* **1986**, *19*, 1494.
(2) Maeda, T.; Fujime, S. *Macromolecules* **1984**, *17*, 2381.
(3) Fujime, S.; Maeda, T. *Macromolecules* **1985**, *18*, 191.
(4) Maeda, T.; Fujime, S. *Macromolecules* **1984**, *17*, 1157.
(5) Doi, M.; Edwards, S. F. *J. Chem. Soc., Faraday Trans. 2*, **1978**, *74*, 560.
(6) Kubota, K.; Chu, B. *Biopolymers* **1983**, *22*, 1461.
(7) Russo, P. S.; Karasz, F. E.; Langley, K. H. *J. Chem. Phys.* **1984**, *80*, 5312.
(8) Pusey, P. N. *J. Phys. A* **1978**, *11*, 119.
(9) Fujime, S.; Maeda, T. In *Physical Optics of Dynamic Phenomena and Processes in Macromolecular Systems*; Sedlacek, B., Ed.; Walter de Gruyter: Berlin and New York, 1985; pp 17-32.
(10) Mori, Y.; Ookubo, N.; Hayakawa, R.; Wada, Y. *J. Polym. Sci.—Phys.* **1982**, *20*, 2111.
(11) Maguire, J. F.; McTague, J. P.; Rondelez, F. *Phys. Rev. Lett.* **1980**, *45*, 1981; correction is in: *Phys. Rev. Lett.* **1981**, *47*, 148.
(12) Zero, K. M.; Pecora, R. *Macromolecules* **1982**, *15*, 87.
(13) Doi, M.; Yamamoto, I.; Kano, F. *J. Phys. Soc. Jpn.* **1984**, *53*, 560.
(14) Teraoka, I.; Mori, Y.; Ookubo, H.; Hayakawa, R. *Rep. Prog. Polym. Phys. Jpn.* **1984**, *27*, 127.
(15) Keep, G. T.; Pecora, R. *Macromolecules* **1985**, *18*, 1167.